Arabian Journal of Chemistry (2022) **15**, 103584

King Saud University

Arabian Journal of Chemistry

www.ksu.edu.sa
www.sciencedirect.com

ORIGINAL ARTICLE

Two new Mn(II) coordination polymers: Photocatalytic property and treatment activity on colorectal cancer by inhibiting cancer cell migration and invasion

RETRACTED

Gang Liu [a,*,1], Yun Huang [a,1], Kunqiu Yang [a], Zhen Cao [a], Zhanwei Zhao [a,*], Chao Wang [b]

[a] *Department of General Surgery, The first Medical Center of PLA General, Beijing, China*
[b] *Department of Applied Chemistry, Inner Mongolia University, Tongliao, Inner Mongolia, China*

Received 18 September 2021; accepted 21 November 2021
Available online 25 November 2021

KEYWORDS

Mn(II) compound;
Photocatalysis;
Colorectal cancer

Abstract Two new binary Mn(II) coordination polymers, namely $[Mn(5\text{-MeO-ip})(DMF)]_n$ (**1**) and $[Mn(obb)]_n$ (**2**) (5-MeO-H_2ip = 5-methoxyisophthalic acid, H_2obb = 4,4′-oxydibenzoic acid), have been synthesized *via* the self-assemble reactions of Mn(II) ions with two different dicarboxylic acid ligands. The optical band gaps for **1**–**2** are 3.21 eV, 3.50 eV, respectively, and their photocatalytic properties for the degradation of MV under UV light irradiation were also investigated. For the colorectal cancer treatment, the biological activity was evaluated and the specific mechanism was explored at the same time. Firstly, the inhibitory activity of the new compounds on the colorectal cancer cell viability was measured with CCK-8 assay. Next, the real time RT-PCR was used to measure the activation of the VEGF signaling pathway in the colorectal cancer cells after compound treatment.
© 2021 The Author(s). Published by Elsevier B.V. on behalf of King Saud University. This is an open access article under the CC BY license (http://creativecommons.org/licenses/by/4.0/).

1. Introduction

Colorectal cancer is one of the malignant tumors with a relatively high incidence. Its incidence rate is among the top five in the world. In the past, the incidence rate in China was relatively low (Haraldsdottir et al., 2014). According to the data released by our current National Cancer Center, the incidence and death rate of colorectal cancer in China are constantly rising. However, the molecular mechanism of the colorectal cancer is not completely clear. (Thanikachalam and Khan, 2019) Therefore, studying the molecular mechanism of the colorectal cancer may provide an experimental basis for the development

* Corresponding authors.
E-mail addresses: liug0921@163.com (G. Liu), zzq194910@163.com (Z. Zhao).
[1] Authors are contributed equally to this work.
Peer review under responsibility of King Saud University.

ELSEVIER Production and hosting by Elsevier

https://doi.org/10.1016/j.arabjc.2021.103584
1878-5352 © 2021 The Author(s). Published by Elsevier B.V. on behalf of King Saud University.
This is an open access article under the CC BY license (http://creativecommons.org/licenses/by/4.0/).

of new molecular targeted therapies for the treatment of colorectal cancer.

In the last several decades, coordination polymers have attracted great interest, which primarily owing to the potential functional properties that make them can be used in the field of sensing, luminescence, gas storage, catalysis, magnetism, drug delivery, etc (Pan et al., 2019; Dutta et al., 2021; Liu et al., 2021; Pan et al., 2020; Li et al., 2020). A lot of research has proved that coordination geometries of metal ion, the structural characteristic, coordination sites of the organic blocks perform as crucial parts in in directing the formation of final structure of the coordination-bond driven self-assembly (Li et al., 2020; Fan et al., 2022). Thus, intelligent selection of structure-related organic blocks and metal ions with specific coordination geometries can help us to obtain the coordination polymers with desired structures and functional properties. Among the various types of organic ligands widely used in the syntheses of coordination polymers, multidentate carboxylate ligands serve as one of the most efficient organic ligands to construct coordination polymers, they display abundant coordination modes and possess high coordination capacities (Fan et al., 2021; Feng et al., 2017; Feng et al., 2015). These carboxylate-based coordination polymers usually exhibit exceptional thermostability and interesting physicochemical properties (Wang et al., 2021; Lu et al., 2021; Zhang et al., 2020). Most of such materials containing Cd(II), Co(II), Cu (II) or Mn(II) ions show promising applications as photocatalysts for the water purification (Li et al., 2021; Sun et al., 2015; Xiao et al., 2019).

Organic dye wastewater is seriously affecting human h[illegible] due to the chemical stability and difficult biodegradabili[illegible] of the organic dyes. In order to protect ecological balance a[illegible]d human health, it is urgent to develop new photo[illegible]lysts wi[illegible] high photocatalytic activities for the photod[illegible]radati[illegible] of th[illegible] organic dyes. Recently, there are various [illegible]pes org[illegible]ic–inorganic hybrid photocatalyst, coordinati[illegible] p[illegible]ym[illegible]s serv[illegible] one type of them, has shown excellen[illegible] photocat[illegible]tic activities, good structure stability and reu[illegible]lity (Kang [illegible]al., 2020; Zhang et al., 2021). To o[illegible]tain [illegible]e new coo[illegible]dination polymer-based photocataly[illegible] we chose [illegible]o different dicarboxylic acid blocks [illegible] this experim[illegible]t, namely 5-methoxyisophthalic ac[illegible] (5-MeO-H$_2$ip) and 4,4′-oxydibenzoic acid (H$_2$obb), that ca[illegible] dopt [illegible]any kinds of bridging or chelating modes linking with [illegible]al ions, t[illegible] assemble with Mn(II) ions under so[illegible]oth[illegible]al co[illegible]ition[illegible] Successfully, we obtained two new M[illegible](II)-ba[illegible]d coordi[illegible]ion polymers formulated as [Mn(5-M[illegible]-ip)(D[illegible]F)]$_n$ (**1**) and [Mn(obb)]$_n$ (**2**). Compound **1** has an ex[illegible]d 3D structure, which has been proven by the structural a[illegible]lyses of X-ray, and compound **2** exhibits an extended 2D lay[illegible]d structure. The thermostability, optical band gaps and photocatalytic activities of both compounds were investigated in this work. In the biological section, the application values of compounds **1** and **2** on the colorectal cancer was measured, followed by the mechanism exploration.

2. Experimental

2.1. Materials and instrumentation

All the raw materials including metal salts, organic ligands, organic solvent are commercially available from Jinan Henghua Company, and there is no need to do further purification. Using a Vario EL-Cube elemental analyzer to do elemental analyses of **1**–**2**. Under the circumstances that a Rigaku Mini-Flex II diffractometer with Cu/Kα radiation (λ = 1.54056 Å) at the scan speed of 2°/minutes and one step size of 0.05°, the powder X-ray diffraction data of 1–2 were gathered. Thermogravimetric analyses were performed on a NETSCHZ STA-449C thermoanalyzer, which at a temperature range from 30℃ to 800℃ under a nitrogen atmosphere. The UV–Vis absorption spectra were collected on the Shimadzu UV–Vis 2501PC recording spectrophotometer.

2.2. Synthesis of [Mn(5-MeO-ip)(DMF)]n (1) and synthesis of [Mn(obb)]n (2)

Sealing the mixture of 5-MeO-I[illegible]p (0.1 mmol[illegible] DMF (2 mL), $MnCl_2{\cdot}4H_2O$ (0.1 mmol) [illegible]ong wi[illegible] H_2O (1 [illegible]L) in the glass vial of 20 ml, then f[illegible]ther heating[illegible] at[illegible] temperature of 110℃ for a day and [illegible]half. W[illegible]n the te[illegible]erature of the mixture was cooled to ro[illegible] te[illegible]erature naturally, colorless block crystals of **1** [illegible]ere gat[illegible]ed in 42[illegible] yield, which relied on $MnCl_2{\cdot}4H_2O$. Anal. Calcd[illegible]%) for $C_{12}H_{13}MnNO_6$ (322.17): C, 44.70; [illegible], 4.[illegible] N, 4.35. F[illegible]nd (%): C, 44.72; H, 4.16; N, 4.37.

[illegible]ture of Mn[illegible]$4H_2O$ (0.1 mmol), H_2obb (0.1 mmol), [illegible]HCO_3 (0.2 mmol) and H_2O (8 mL) was sealed in the glass [illegible]al of 20 ml, [illegible]en further heating it at 110℃ for 3 days. When [illegible]e temperatu[illegible] of the mixture was cooled to room temperatu[illegible]at a rat[illegible] of 2℃/min, colorless block crystals of **2** were gathe[illegible] 38% yield relied on $MnCl_2{\cdot}4H_2O$. Anal. Calcd. [illegible]) for $C_{14}H_8MnO_5$ (311.14): C, 53.99; H, 2.57. Found (%): C, 54.02; H, 2.55.

2.3. X-ray crystallography

Choosing proper single crystals of **1**–**2,** mounting it on a glass fiber under an optical microscope. The single crystal data of **1**–**2** was gathered on the Rigaku Mercury CCD diffractormeter, which is controlled by computer and equipped with graphite–monochromated Mo–*K*α radiation (λ = 0.71073 Å) at room temperature. The single crystal data reduction was performed by the CrysAlisPro, and the empirical absorption corrections were performed by the SADABS program (Sheldrick, 1996). Using the procedure of SHELXS-2014, via the direct method solve the structures of **1**–**2**, and refine them via full matrix least-squares, which is based on F^2 (Sheldrick, 2015). To refine all non-hydrogen atoms, anisotropic thermal parameters was performed, and adding all hydrogen atoms bonded to carbon geometrically, then using a riding model to refine isotropically. As we can see from the Table 1, there has summarized the detailed data of the crystallographic and structural refinements of the compounds. Chosen bond lengths (Å) and angles (°) of the compounds were given in Table S1.

2.4. Photocatalytic experiments

Based on the previously reported literature (Yuan et al., 2020), the procedure of photocatalytic experiment conducted in this work is as follows: the finely grind samples of **1** or **2** (50 mg) was added into 100 mL methyl violet (MV) aqueous solution with the concentration of 10 mg/L, and the suspension was fur-

RETRACTED

Table 1 The structure refinements and Crystal data of compounds 1–2.

Sample	1	2
Formula	$C_{12}H_{13}MnNO_6$	$C_{14}H_8MnO_5$
Fw	322.17	311.14
Crystal system	orthorhombic	monoclinic
Space group	$Pna2_1$	$P2/c$
a (Å)	7.437(3)	13.225(2)
b (Å)	15.164(7)	10.9116(14)
c (Å)	11.278(5)	4.8224(6)
α°	90	90
β°	90	95.118(10)
γ°	90	90
Volume (Å^3)	1271.9(10)	693.13(17)
Z	4	2
Density (calculated)	1.683	1.491
Abs. coeff. (mm^{-1})	1.063	0.966
Total reflections	9331	5255
Unique reflections	2851	1564
Goodness of fit on F^2	1.003	1.104
Final *R* indices	R = 0.0234,	R = 0.0632,
[I > 2sigma(I^2)]	wR_2 = 0.0460	wR_2 = 0.1772
R (all data)	R = 0.0265,	R = 0.0754,
	wR_2 = 0.0473	wR_2 = 0.1956
CCDC	2,109,418	2,109,419

ther stirred under the circumstances of darkness for half an hour to establish a balance between adsorption and desorption equilibrium. Then, a photocatalytic reaction was carried out through the XPA-7 type photochemical reactor, which is fitted with 100 W mercury lamp. At the given intervals, taking out 5.0 mL mixture, separating it via centrifugation, and analysing it through UV–vis spectrometer subsequently. Under the same reaction environment, a blank test was also performed without any photocatalyst.

2.5. CCK-8 assay

The CCK-8 assay was conducted in this present research to measure the inhibitory activity of compounds **1** and **2** on the colorectal cancer viability. This reformation was conducted totally under the guidance of the instructions with only a little change. In brief, CT-26 colorectal cancer cells in the logical growth phage were collected and seeded into the 96 well plates (5000 cells/well). The cells were placed in the incubator of 37℃, 5 %CO_2 for 12 h. 48 h after incubation, compounds **1** and **2** were added into the wells with 0–80 μM. Then, the cell culture medium was discarded and the fresh medium was added containing 10 μL CCK-8 reagent. After the indicated treatment, the absorbance of each well was measured at 450 mm. This experiment was repeated at least three times, and the results were presented as mean ± SD.

2.6. Real time RT-PCR

The real time RT-PCR was conducted in this present research to measure the activation of the VEGF signaling pathway in the CT-26 colorectal cancer cells after compounds treatment. This conduction was finished strictly in accordance with the instructions. Shortly, the PC-1 pancreatic cancer cells in the logical growth phage were collected and seeded into the 6 well plates at the final destiny of 10^6 cells/ well. The cells were placed in the incubator of 37℃, 5 %CO_2 for 12 h, then the new compounds were added for treatment with indicated concentrations. Next, the cells were collected and the total RNA in the cells were extracted with TRIZOL reagent. After measuring the concentration of the total RNA, which was then reverse transcripted into cDNA. The relative expression of the VEGF signaling pathway in the CT-26 colorectal cancer cells was measured with real time RT-PCR, the *gapdh* was used as the internal control gene. This experiment was repeated at least three times, and the results were presented as mean ± SD.

3. Results and discussion

3.1. Crystal structure of 1

As we can see from the X-ray crystallographic analysis, the compound **1** crystallizes in the orthorhombic $Pna2_1$ space group and is a extended 3D structure relied on 1D Mn-carboxylate chains. In the asymmetric unit of **1**, there are one Mn(II) ion, one 5-MeO-ip^{2-} ligand and one terminal coordinated DMF molecule. The Mn1 ion is five-coordinated by four carboxylate oxygen atoms from four different 5-MeO-ip^{2-} ligands, and one oxygen atom from terminal coordinated DMF molecule, affording a trigonal bipyramid of {MnO_5} with the Mn-O distances at the range of 2.115(2)-2.210(2) Å (Fig.). The carboxylate group of each 5-MeO-ip2- ligand are in uniform bis-monodentate model. As shown in Fig. 1b, adjacent {MnO_5} polyhedrons are bis-bridged by two bis-monodentate carboxylate groups, thus leading to the formation of a 1D Mn-carboxylate chain subunit extending along *a* axis, and in this 1D chain, the neighboring distance of Mn. . .Mn is 3.82 Å. Finally, these 1D chains are further linked by the 5-MeO-ip^{2-} ligands to form an extended 3D structure for **1** (Fig. 1c). After remove the coordinated DMF molecules, it can be observed that the solvent-free framework for 1 contains 1D opened channels running along crystallographic *a* axis (Fig. 1d), and the solvent-accessible volume is 29.4% calculated by the PLATON program.

3.2. Crystal structure of 2

The crystal structure of **2** is an extended 2D layer crystallizing in the monoclinic $P2/c$ space group with its asymmetric unit consisting of a half Mn(II) ion and a half obb^{2-} ligand. Fig shows that, six carboxylate oxygen atoms formed the Mn1 ion, which locates in the center of a slightly distorted octahedron, these carboxylate oxygens are offered by six different obb^{2-} blocks. The bond lengths of Mn-O are ranging from 2.121(3) to 2.297(3) Å. The V-shaped dicarboxylate ligand of obb^{2-} adopt a (κ^1-μ_2)-(κ^1-μ_2)-μ_6 coordination mode with its two deprotonated carboxylate groups linking six different Mn(II) ions. It is worth noting that the connection between adjacent Mn ions is four-bridged by the carboxylate groups of obb^{2-} ligands, which results in the formation of 1D Mn (II)-carboxylate chain running along crystallographic *c* axis (Fig. 2b). The 2-connected obb^{2-} ligands further connected these 1D Mn(II)-carboxylate chains into an extended 2D layer (Fig. 2c). Viewing along crystallographic *c* axis, 1D opened

RETRACTED

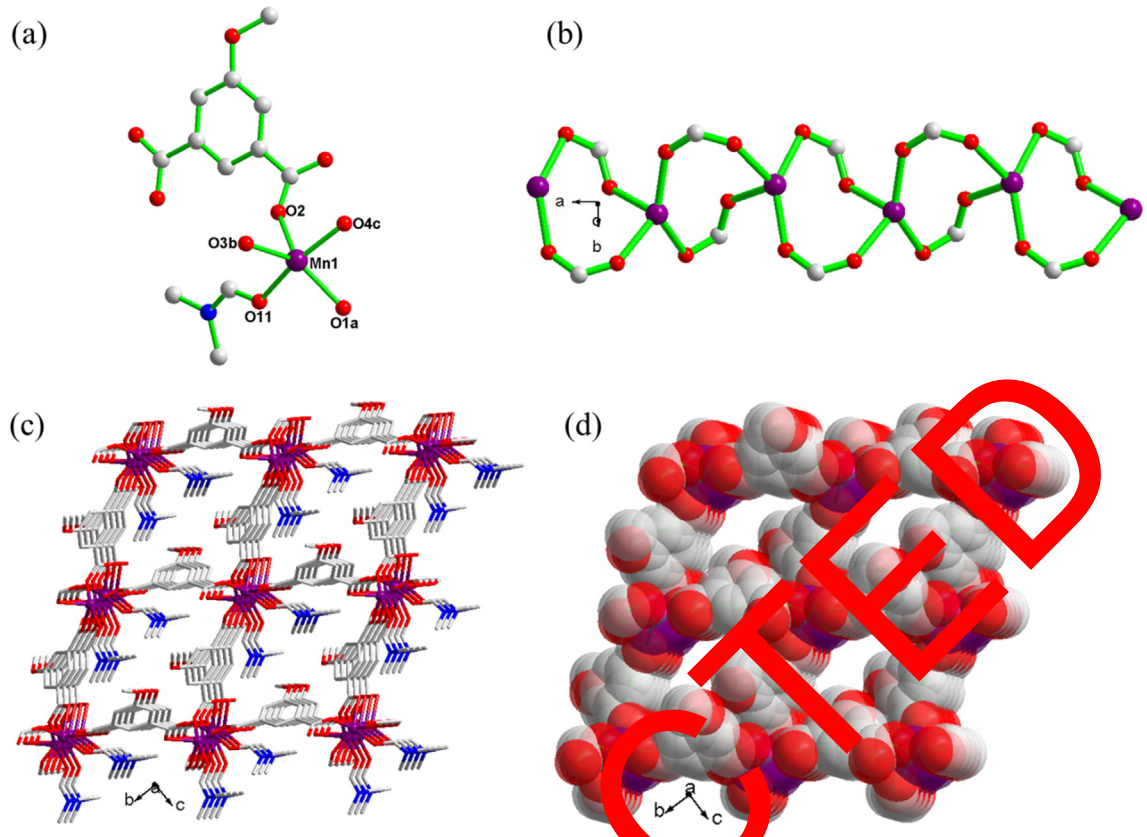

Fig. 1 (a) Viewing of the coordination environment of Mn[illegible]ion in **1**. (b) [illegible]Mn(II)-carboxylate chain structure. (c) The extended 3D structure of 1. (d) The 3D porous structure for 1 after re[illegible]ving the coordinated DMF molecules.

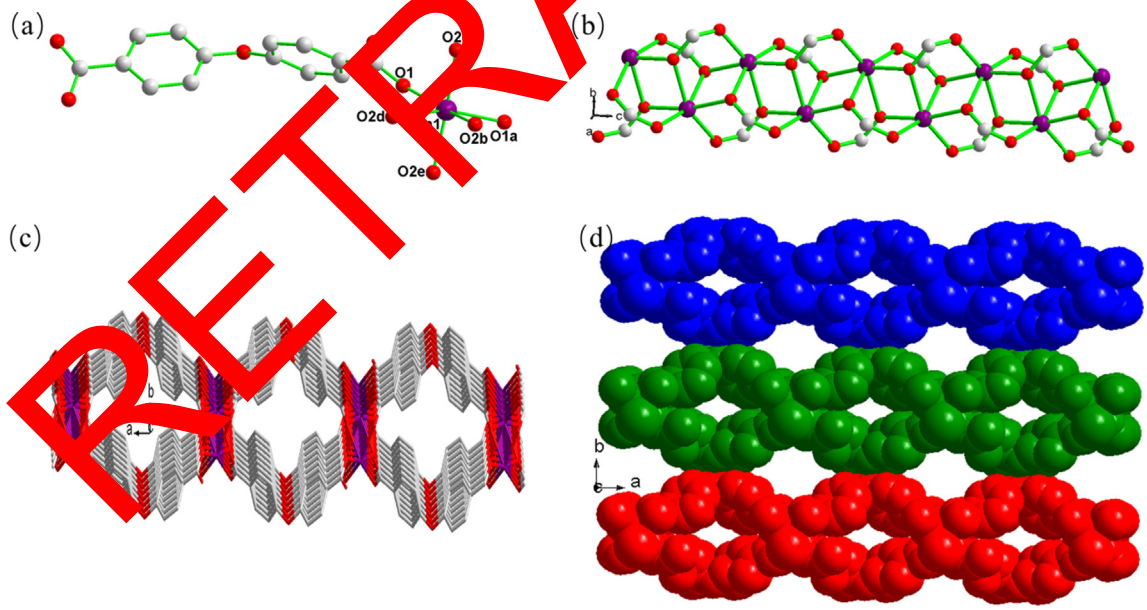

Fig. 2 (a) Viewing of the coordination environment of Mn(II) ion in **2**. (b) The 1D Mn(II)-carboxylate chain structure in **2**. (c) The extended 2D layered structure of **2** with 1D opened channels viewing along crystallographic *c* axis. (d) The layer-to-layer stacked 3D supramolecular framework under weak Van der Waals interactions.

channels in such 2D layer can be observed. Further, the final 3D supramolecular structure (Fig. 2d) was formed by the weak Van der Waals force-induced stacking of these 2D layers in -AA- mode. As calculated by the PLATON program, the solvent-accessible volume for **2** is 121.7 $Å^3$, corresponding to 17.6% of the unit cell volume.

RETRACTED

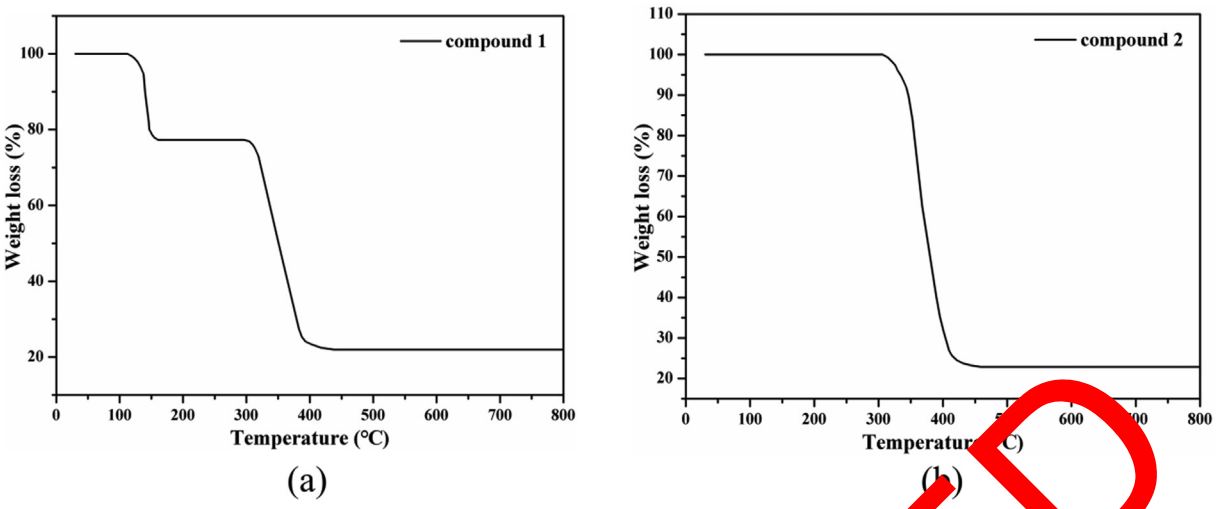

Fig. 3 The TGA curves (a) for **1** and (b) for **2**.

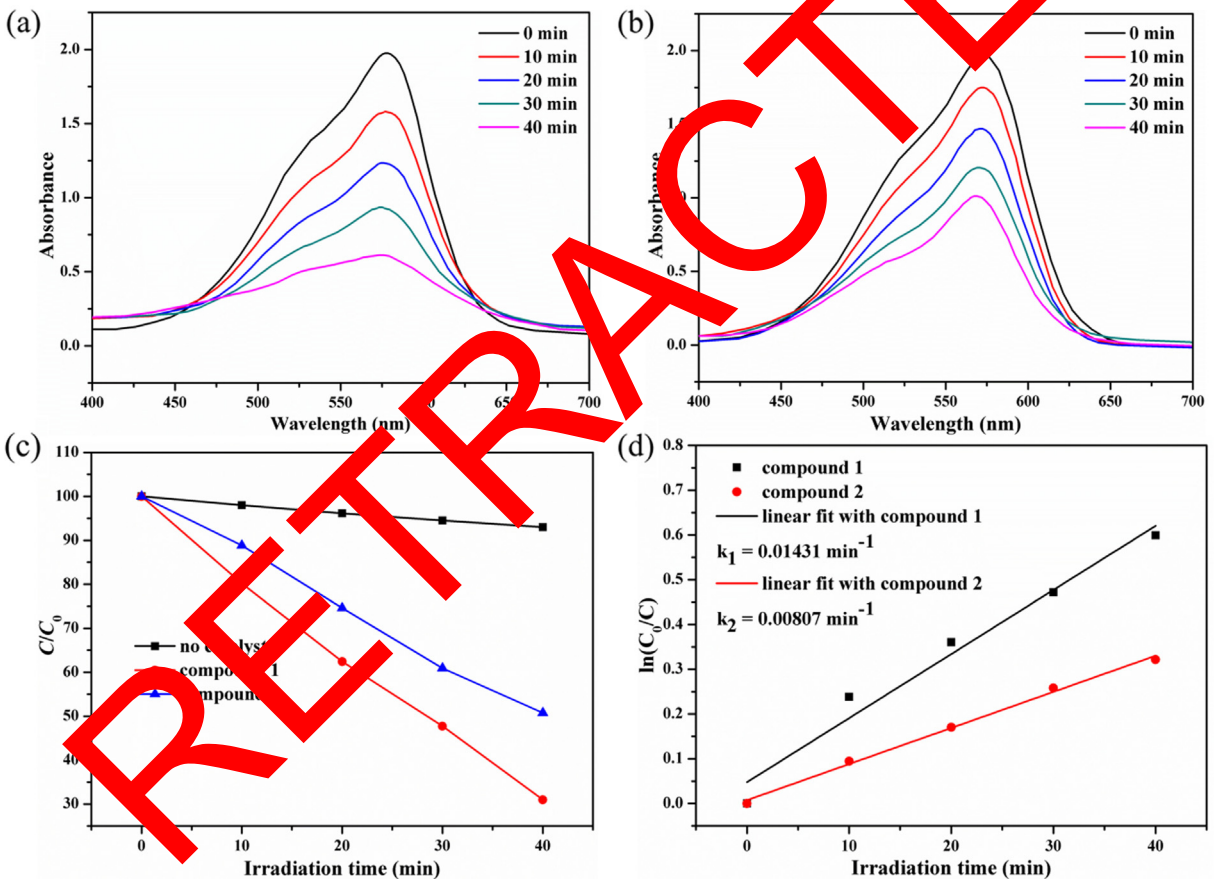

RETRACTED

Fig. 4 (a) The UV–Vis absorption spectra of MV solution in the presence of **1** under different irradiation time. (b) The UV–Vis absorption spectra of MV solution in the presence of **2** under different irradiation time. (c) The plots of C/C_0 versus irradiation time. (d) The first-order kinetic plots of photodegradation MV under the circumstances of the presence of compound **1** and compound **2**.

3.3. TGA and PXRD patterns

The experiments of PXRD were conducted to verify whether the as-synthesized samples of **1**–**2** are in pure phase. Fig shows that, S1, the PXRD patterns of **1**–**2** based on the synthesized samples fits nicely with their corresponding simulated patterns relied on the data of single crystal diffraction, clearly suggesting that the bulk samples of **1**–**2** are in single phase.

Furthermore, through the thermogravimetric analysis tests under N_2 atmosphere (Fig. 3), their thermal stabilities were

investigated at the same time. The significant two steps weightlessness were shown by the TGA curve of **1**: one is appeared in the range of 112-160℃ with a weight loss of 22.65% because of the evaporation of the coordinated DMF molecules (calcd: 22.69%), the other occurred in the temperature range of 295–417 ℃, the decomposition of the organic ligand (calcd: 55.25%) lead to a weight loss of 55.36%. The TGA curve of **2** indicated that no observed weight loss took place before 306℃, and after that, the collapse of the framework was observed and weight loss continued to 458℃ due to the loss of the organic ligand.

3.4. Band gaps and photocatalytic properties of 1–2

The UV–Vis absorption spectra of **1**–**2** as well as free organic ligands of 5-MeO-H_2ip and H_2obb were measured at room temperature (Fig. S2a). As calculated by the Kubelka-Munk (K-M) function of $F_R = (1–R)^2/2R$ (R: the diffuse reflectance of the samples) based on the UV–vis absorption data, the band-gap energies (E_g) are 3.21 eV for **1** and 3.50 eV for **2** (Fig. S2b), indicating that such two compounds may be served as good photoactive materials in the field of photocatalysis.

Furthermore, the methyl violet (MV) was selected as a model dye contaminant to evaluate the photocatalytic activities of **1**–**2**. And the blank experiment in the absence of photocatalyst was also performed under the same conditions. As shown in Fig. 4a and 4b, the absorption peaks of MV solution under the circumstances of the presence of compounds **1**–**2** declined gradually when exposing the UV light from 0 min to 40 min, and after 40 min, the degradation efficiencies of MV solution reached to 69.12%, 4[illegible] respectively, in the presence of **1**–**2** (Fig. 4c). The [illegible]gradation [illegible]fficiency of **1** is much higher than previous lite[illegible]ture MOFs f[illegible] MV degradation under the similar co[illegible]dition[illegible] (Table 2). However, the

Table 2 Performances of some MOFs as photocatalysts for the degradation of MV [illegible] aqu[illegible] media.

MOF	Irradiation	Time (min)	[illegible]egradation e[illegible]ienc[illegible]%)	Ref
$\{[Zn_4(NDC)_{3.5}(\mu_4\text{-OH})(DMF)]\cdot 1.7DMF\}_n$	UV–vis	45	78[illegible]	Pan et al., 2019
$[Co_2(1,4\text{-bdc})(ncp)_2]$	Vis	300	33.29	Sun et al. (2013)
$[Cd(L)(Hbpz)]_n$	UV	35	47.2	Cai et al. (2019)
$\{[Zn(L)(4,4'\text{-bipy})\cdot CH_3CN]_n$	UV	100	60.6	Wu et al. (2017)
$\{[Co_2(bdc)_2(bmp)_{1.5}]\cdot DMF\cdot 1.5H_2O\}_n$	UV	40	[illegible]	Zhou et al. (2020)
1	UV	40	6[illegible]12	This work

RETRACTED

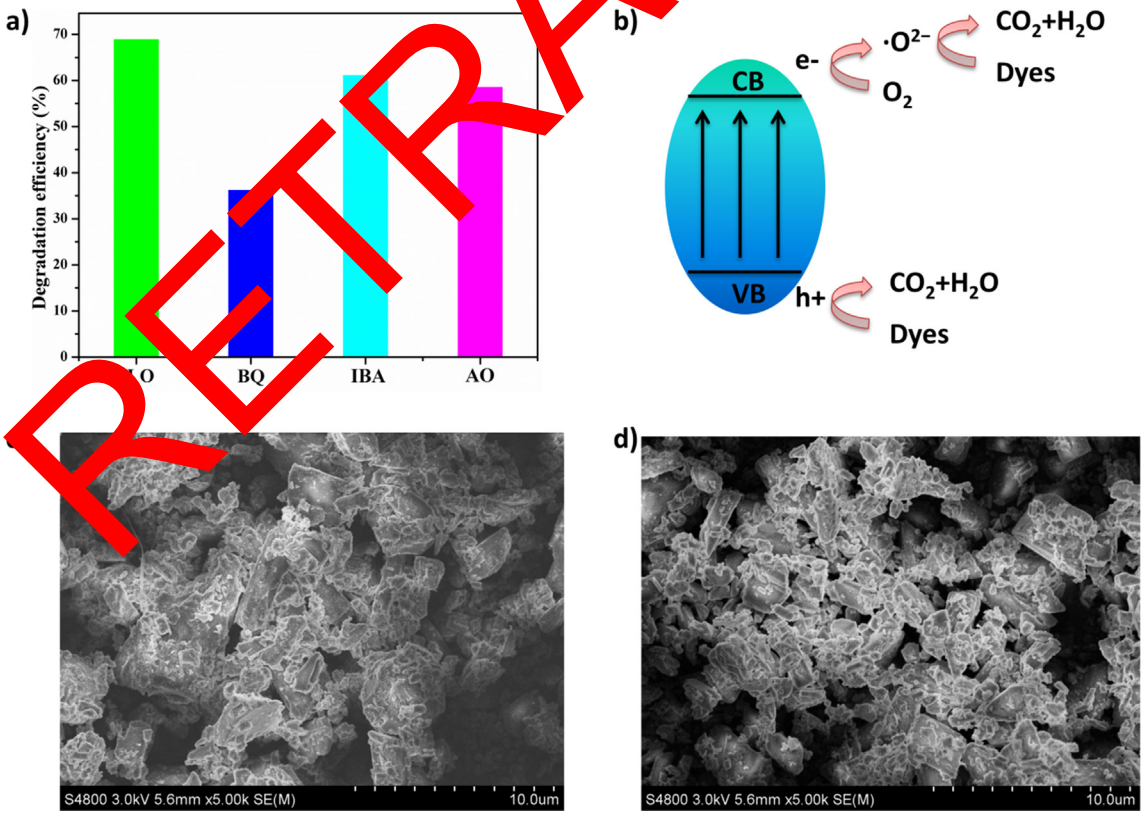

Fig. 5 (a) Photodegradation efficiency of MV solution in the presence of **1** along with different scavengers (BQ, IBA and AO). (b) The possible photodegradation mechanism of **1**. The SEM diagrams of **1** before (c) and after (d) photodegradation experiments.

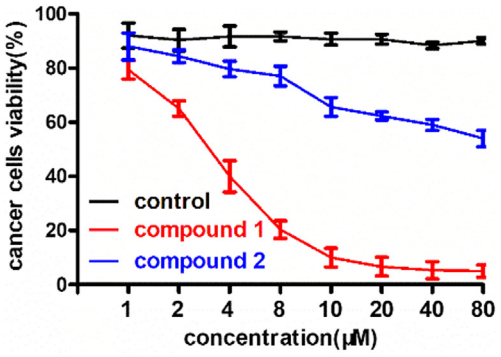

Fig. 6 Significantly reduced viability of the CT-26 colorectal cancer cells after compound treatment. The CT-26 colorectal cancer cells in the logical growth phage were collected and seeded into the cell culture plate, then compounds **1** and **2** were added for treatment with serial different dilutions. The viability of the CT-26 colorectal cancer cells was measured with CCK-8 assay.

degradation efficiency of MV solution in the absence of photocatalyst reduced to 7.65% after 40 min UV light irradiation (Fig. 4c). This indicates that compounds **1**–**2** can be used as photocatalysts for the degradation of MV under UV light irradiation. It is noteworthy that the degradation efficiency of MV in the presence of **1** is higher than that in the presence of **2**, suggesting that the photocatalytic performance of **1** is better than that of **2**.

In addition, the degradation reaction rate constants with compounds as photocatalysts were also calculated using the model of pseudo-first-order kinetic: ln(C0/C) = kt (C0: the initial concentration of MV, C: the concentration of MV at irradiation time t, k: the fitted first-order rate constant). As we can see from the Fig. 4b, there has a linear relationship between the plots of ln(C0/C) and t, and the linear fittings give the rate constants of 0.01431 min^{-1} for **1**, 0.00807 min^{-1} for **2**. The rate constant of **1** is higher than that of **2**, which is in the same of the sequence of degradation efficiencies, further demonstrating that the better photocatalytic activity of **1** than **2**.

The possible photocatalytic mechanism was also explored *via* the trapping experiments by selection of **1** as the representative (Zhao et al., 2019). Herein, various scavengers, such as benzoquinone (BQ) as a O_2^- scavenger, isopropanol (IBA) as a ·OH scavenger, ammonium oxalate (AO) as a h^+ scavenger, were used to explore the active species in the photodegradation reaction. When using the IBA and AO as the scavengers, the degradation efficiencies of MV were slightly decreased from 69.12% to 61.3%, 58.7%, respectively (Fig. 5). However, the degradation efficiency of MV was significantly reduced from 69.12% to 36.4% using the BQ scavenger (Fig. 5a). This result indicates that O_2^- was the dominated active species during the photocatalytic process with **1** as photocatalyst. In general, the mechanism of photocatalytic degradation of dye using MOFs as catalysts is associated with semiconductor theory. Previous studies have suggested that the electron charge transfer from the photoexcited organic ligand to the metal (LMCT) within MOFs account for their photocatalytic activity. Thus, the mechanism of dye degradation of **1** can be proposed as shown in Fig. 5b. When **1** is irradiated with photons, electrons are excited from the valence band (VB) to the conduction band (CB), accompanied by formation of positive-charged holes (h^+) in the VB. Degradation of dye molecules will be mediated by the strongly oxidizing holes (h^+). At the same time, superoxide radicals ($O_2^{\cdot-}$) formed by the reaction of electrons with oxygen will also have a strong ability to oxidize dye molecules. In addition, we have also recorded the scanning electron microscope (SEM) diagrams of complex **1** before and after photocatalytic reactions, and it could be observed that its morphology does not obviously change, indicating the catalyst **1** does not decompose (Fig. 5c and Fig. 5d).

RETRACTED

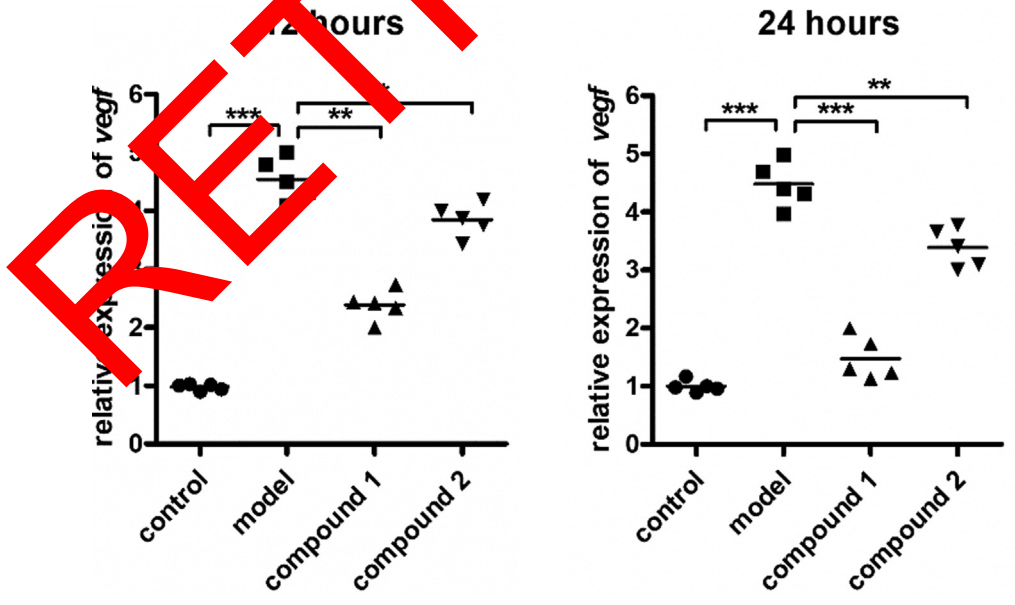

Fig. 7 Regulated VEGF signaling pathway signaling pathway in the CT-26 colorectal cancer cells after compound treatment. The PC-1 pancreatic cancer cells in the logical growth phage were collected, then the compound was added for treatment at indicated different concentrations. The real time RT-PCR was recommended to measure the VEGF signaling pathway signaling pathway in the CT-26 colorectal cancer cells.

3.5. Compound significantly reduce the viability of the CT-26 colorectal cancer cells

After the design and synthesis of the new compounds **1** and **2** with novel structures, their treatment activity on the CT-26 colorectal cancer cells viability was determined. So, the CCK-8 assay was carried out in this research, and the viability of CT-26 colorectal cancer cells after compound treatment was measured. As the results showed in the Fig. 6, we can see there was a higher level of CT-26 colorectal cancer cells viability in the control group. After the treatment of compound **1**, the CT-26 colorectal cancer cells viability was reduced significantly, which is significantly different from the control group, with $P < 0.005$. However, compound **2** only showed a little influence on the viability of the CT-26 colorectal cancer cells, which was much weaker than compound **1**.

3.6. Compound reduced the VEGF signaling pathway activation in the CT-26 colorectal cancer cells

As we proved in the above experiment, the new compound showed excellent inhibitory activity on the viability of CT-26 colorectal cancer cells. As previously reported, the VEGF signaling pathway in the CT-26 colorectal cancer cells play an important role in the development of colorectal cancer cells. Thus, the real time RT-PCR was further conducted and the activation of the VEGF signaling pathway in the CT-26 colorectal cancer cells was measured. The results in Fig. 7 showed that there was a significantly increased level of VEGF signaling pathway in the CT-26 colorectal cancer cells compared with the normal cells. There was obviously difference between these two groups, with $P < 0.005$. Under the treatment of the new compound, the relative expression of the VEGF signaling pathway in the CT-26 colorectal cancer cells was reduced significantly, which is much more excellent than compound **2**.

4. Conclusions

In summary, two new Mn(II)-based coordination polymers have been prepared based on two different dicarboxylic acid ligands. Owing to different molecular structures of the dicarboxylic acid ligands, **1** shows an extended 3D framework, and **2** shows an extended 2D layered structure. Moreover, both them have been tested with the optical band gaps of 2.31 eV and 2.50 eV, and the photocatalytic degradation efficiencies for **1**–**2** are 69.12% and 49.17% respectively, after 40 min UV light irradiation. The CCK-8 assay indicated that compound **1** was more excellent than compound **2** on inhibiting the colorectal cancer cell viability. Next, the activation of the VEGF signaling pathway in the colorectal cancer cells was obviously reduced by compound **1**, but not compound **2**. Above all, we got this conclusion that compound **1** was much better than compound **2** on the colorectal cancer treatment through inhibiting the cancer cell viability, migration and invasion ability.

Data availability

Selected bond lengths (Å) and angles (°) for CPs **1**–**2** (Table S1); The PXRD patterns (a) for **1** and (b) for **2** (Fig. S1); (a) The UV–Vis absorption spectra for compounds and free dicarboxylic acid ligands. (b) The diffuse reflectance spectra of K–M function versus energy for **1**–**2** (Fig. S2), the information could be found in the supporting information file.

Declaration of Competing Interest

The authors declare that they have no known competing financial interests or personal relationships that could have appeared to influence the work reported in this paper.

Acknowledgments

Not applicable.

Funding

Not applicable.

Appendix A. Supplementary material

Supplementary data to this article can be found online at https://doi.org/10.1016/j.arabjc.2021.103584.

References

Cai, S.L., Lu, L., Wu, W.P., Wang, J., Sun, Y.C., Ma, A.Q., Singh, A., Kumar, A., 2019. A new mixed ligand based Cd(II) 2D coordination polymer with functional sites: Photoluminescence and photocatalytic properties. Inorg. Chim. Acta 484, 291–296.

Dutta, A., Pan, Y., Liu, J., Kumar, A., 2021. Multicomponent particular metal-organic frameworks: Principles, current status and challenges. Coord. Chem. Rev. 445, 214074.

Fan, L., Zhao, D., Zhang, H., Wang, F., Li, B., Yang, L., Deng, Y., Zhang, X., 2021. A hydrolytically stable amino-functionalized Zinc (II) metal-organic framework containing nanocages for selective gas adsorption and luminescent sensing. Micropor. Mesopor. Mat. 326, 111396.

Fan, L., Zhao, D., Li, B., Wang, F., Deng, Y., Peng, Y., Wang, X., Zhang, X., 2022. Luminescent binuclear Zinc(II) organic framework as bifunctional water-stable chemosensor for efficient detection of antibiotics and Cr(VI) anions in water. Spectrochim. Acta A 264, 120232.

Feng, X., Li, R.F., Wang, L.Y., Ng, S.W., Qin, G.Z., Ma, L.F., 2015. A series of homonuclear lanthanide coordination polymers based on a fluorescent conjugated ligand: syntheses, luminescence and sensor. CrystEngComm 17, 7878–7887.

Feng, X., Feng, Y.Q., Guo, N., Sun, Y.L., Zhang, T., Ma, L.F., Wang, L.Y., 2017. Series d−f heteronuclear metal−organic frameworks: color tunability and luminescent probe with switchable properties. Inorg. Chem. 56, 1713–1721.

Haraldsdottir, S., Einarsdottir, H.M., Smaradottir, A., Gunnlaugsson, A., 2014. Halfdanarson TR. Colorectal cancer - review. Laeknabladid 100, 75–82.

Kang, W.C., Hao, Z.C., Han, C., Dong, G.Y., 2020. Multicomponent self-assembly of two Cd(II)-based coordination polymers: synthesis, structures and photocatalytic properties. J. Inorg. Organomet. Poly. 30, 1877–1885.

Li, G.L., Yin, W.D., Liu, Q.L., Gong, X.R., Zhao, Y.J., Liu, G.Z., 2021. N-donor-induced two Co(II) coordination polymers derived from the flexible citraconic acid as photocatalysts for the decomposition of organic dyes. Z. Anorg. Allg. Chem. 647, 1–9.

Li, R.F., Zhang, Y.W., Liu, X.F., Chang, X.H., Feng, X., 2020. The synthesis, structural elucidation and fluorescent sensitization detec-

RETRACTED

tion to Hg^{2+} based on two lanthanide-organic complexes. Inorg. Chim. Acta 502, 119370.

Li, R.F., Li, R.H., Liu, X.F., Chang, X.H., Feng, X., 2020. Lanthanide complexes based on a conjugated pyridine carboxylate ligand: structures, luminescence and magnetic properties. RSC Adv. 10, 6192–6199.

Liu, W., Pan, Y., Zhong, Y., Li, B., Ding, Q., Xu, H., Qiu, Y., Ren, F., Li, B., Muddassir, M., Liu, J., 2021. A multifunctional aminated UiO-67 metal-organic framework for enhancing antitumor cytotoxicity through bimodal drug delivery. Chem. Eng. J. 412, 127899.

Lu, L., Wang, J., Shi, C.Y., Jiang, X., Sun, Y., Wu, W., Hu, W., 2021. Four new coordination complexes prepared for the degradation of methyl violent dye based on flexible dicarboxylate and different N-donor coligands. J. Mol. Struct. 1225, 129181.

Pan, Y., Ding, Q., Xu, H., Shi, C., Singh, A., Kumar, A., Liu, J., 2019. A new Zn(ii)-based 3D metal–organic framework with uncommon **sev** topology and its photocatalytic properties for the degradation of organic dyes. CrystEngComm 21, 4578–4585.

Pan, Y., Luo, Z., Wang, X., Chen, Q., Chen, J., Guan, Y., Liu, D., Xu, H., Liu, J., 2020. A versatile and multifunctional metal–organic framework nanocomposite toward chemo-photodynamic therapy. Dalt. Trans. 49, 5291–5301.

Sheldrick, G.M., 1996. SADABS. University of Göttingen, Göttingen, Germany.

Sheldrick, G.M., 2015. Acta Crystallogr. Sect. C: Struct. Chem. 71, 3–8.

Sun, H.Y., Liu, C.B., Cong, Y., Yu, M.H., Bai, H.Y., Che, G.B., 2013. New photocatalyst for the degradation of organic dyes based on $[Co_2(1,4\text{-BDC})(NCP)_2]n{\cdot}4nH_2O$. Inorg. Chem. Commun. 35, 130–134.

Sun, Y.Q., Zhong, J.C., Ding, L., Chen, Y.P., 2015. Syntheses, structures, photoluminescence and photocatalysis of chiral 3D Cd (II) frameworks from achiral mixed flexible ligands by spontane resolution. Dalt. Trans. 44, 11852–11859.

Thanikachalam, K., Khan, G., 2019. Colorectal Cancer and Nutrition. Nutrients 11, 164.

Wang, X.F., Guo, X.Y., Liu, T., 2021. Two Co(II) based coordination polymers constructed from π-electron-rich polycarboxylate aryl ether ligand: structural insights and photocatalytic dye degradation. Chin. J. Struct. Chem. 40, 722–728.

Wu, Y., Feng, J., Xie, B., Zou, L., Li, Y., Li, Z., 2017. An Extremely Stable 2D Zinc(II) Coordination Polymer Exhibiting High Sensing Ability and Photocatalytic Degradation Activities of Dyes. J. Inorg. Organomet. Polym. Mater. 27, 1243–1251.

Xiao, Q.Q., Liu, D., Wei, Y.L., Cui, G.H., 2019. Two new ternary Mn (II) coordination polymers by regulation of aromatic carboxylate ligands: Synthesis, structures, photocatalytic and selective ion-sensing properties. J. Solid State Chem. 273, 67–74.

Yuan, F., Yu, H.S., Yuan, C.M., Zhou, C.S., [illegible] F., Lu, Y.J., Ling, X. Y., Wang, J., Singh, A., Kumar, A., 202[illegible] Structures and photocatalytic properties of two M[illegible](II)-based coordination polymers. Inorg. Chim. Acta 499, 119[illegible]

Zhang, D., Bi, C., Zong, Z., [illegible], Y., 2020. Three different Co(II) metal–organic framework based on 4,[illegible]bis(imidazolyl)diphenyl ether: syntheses, crystal structure and photocatalytic properties. J. Inorg. Organomet. Po[illegible]30, 5[illegible]5–5156.

Zhang, Y., Hu, X., [illegible]o, C., [illegible], D., Hu[illegible], Jin, J., Muddassir, M., 2021. Fast photocatalytic organic dye by two metal-organic framework[illegible] 3D two-fold interpenetrated feature. J. Mol. Struct. 1227, 129[illegible]

Zhao, R.Y., Xu, R.D., [illegible] G.N., Sun, Y., Li, C., 2019. Water stable tetranuclear copper(I) iodide cluster for visible-light driven photocatalytic application. Inorg. Chem. Commun. 105, 135–139.

Zh[illegible]u, E.H., Hu[illegible]V., Ding, Q., Li, L., Liao, Z., Jin, J.C., 2020. Photocatalytic decontamination of methyl violet by a 3D twofold interpenetrating metal–organic framework. Inorg. Chem. Commun. [illegible]8155.

RETRACTED